ORIGINAL ARTICLE



Developing a novel reference region for [18F]PI-2620-PET imaging to facilitate the assessment of 4-repeat tauopathies

Lukas Frontzkowski^{1,2} · Johannes Gnörich² · Mattes Gross^{1,2} · Amir Dehsarvi¹ · Sebastian N. Roemer-Cassiano^{1,3} · Carla Palleis^{3,4,5} · Sabrina Katzdobler³ · Anna Dewenter¹ · Anna Steward¹ · Davina Biel¹ · Fabian Hirsch¹ · Zeyu Zhu¹ · Johannes Levin^{3,4,5} · Andrew W. Stephens⁶ · Andre Müller⁶ · Norman Koglin⁶ · Gérard N. Bischof⁶ · Gabor G. Kovacs^{7,8} · Günter U. Höglinger^{3,4,5} · Matthias Brendel^{2,4,5} · Nicolai Franzmeier^{1,4,9}

Received: 9 April 2025 / Accepted: 31 May 2025 / Published online: 10 June 2025 © The Author(s) 2025

Abstract

Purpose Progressive supranuclear palsy (PSP) is a fatal 4-repeat (4R) tauopathy with progressive movement phenotypes. In-vivo 4R tau biomarkers are therefore crucial for PSP diagnosis, monitoring, and treatment evaluation. The tau-PET tracer [¹⁸F]PI-2620 binds to 4R tau and shows increased uptake in PSP-associated regions (e.g., globus pallidus), and is therefore a candidate 4R tau biomarker. However, commonly used cerebellar tau-PET reference regions show regional proximity to cerebellar 4R tau deposits in PSP, confounding semiquantitative [¹⁸F]PI-2620 assessments. Therefore, we employed bias-free image-derived input function (IDIF) PET quantification to identify an optimized data-driven reference region for assessing 4R tau in PSP.

Methods Dynamic [18 F]PI-2620 PET (60 min) was acquired in 58 PSP-Richardson Syndrome (PSP-RS) and 18 healthy controls (HC). IDIF-modelling with carotid timeseries derived total distribution volume (VT). Iteratively normalizing VT images to atlas-based white matter (WM), we identified reference candidates maximizing PSP-RS vs. HC pallidum differences. The best-performing WM references were combined to a temporo-orbital WM reference, validated in PSP-nonRS (n = 54), HC (n = 18), and disease controls (α-synucleinopathies, n = 21; Alzheimer's disease (AD, n = 22) using VT-ratios (VTr) and 20-40min static standardized uptake value ratios (SUVr).

Results Using the data-driven temporo-orbital WM reference, PSP patients showed significantly higher basal ganglia [¹⁸F] PI-2620 signal vs. HC compared to cerebellar normalization. Receiver operating curve (ROC) analysis confirmed higher diagnostic accuracy using the temporo-orbital WM reference. Pallidum [¹⁸F]PI-2620 showed significant associations with clinical disease severity exclusively when using the novel temporo-orbital WM reference.

Conclusions A data-driven temporo-orbital WM reference optimizes [¹⁸F]PI-2620 PET assessment for PSP diagnosis, outperforming conventional cerebellar references used in tau-PET imaging.

Keywords Tau · [¹⁸F]PI-2620 · Progressive supranuclear palsy · Four-repeat tauopathies · Reference region

Abbreviations		SUVr	Standardized Uptake Value Ratio
PSP-RS	Progressive supranuclear palsy with Rich-	VTr	Total Volume Of Distribution Ratio
	ardson syndrome	ROC	Receiver operating curve
PSP-nonRS	Progressive supranuclear palsy with other	ROI	Region Of Interest
	phenotype than Richardson syndrome	GM	Grey Matter
IDIF	Image-Derived Input Function	WM	White Matter

Lukas Frontzkowski, Johannes Gnörich, and Mattes Gross contributed equally as first authors.

Matthias Brendel and Nicolai Franzmeier contributed equally as senior authors.

Extended author information available on the last page of the article



Introduction

Neurodegenerative 4-repeat (4R) tauopathies are characterized by cerebral 4R tau accumulation, leading to progressive motor and cognitive dysfunction [1–4]. The most common manifestations of 4R tauopathies are progressive supranuclear palsy (PSP) with Richardson syndrome (PSP-RS) and cortico-basal syndrome (CBS), both of which share clinical similarities with the α-synucleinopathy Parkinson's disease (PD) or the secondary 3/4R tauopathy atypical Alzheimer's disease (AD) [5, 6]. Currently, the diagnosis of PSP is based purely on clinical criteria, with definitive confirmation only post-mortem, as no sensitive and specific in vivo biomarkers are clinically established, which hinders molecularly defined in vivo identification of PSP pathology [7–10]. Recent advances in tau-PET imaging have drastically improved the detection of tau in the secondary 3/4R tauopathy AD, which has transformed biomarker-based diagnosis, staging, prognosis and treatment monitoring in AD [11, 12]. However, 1 st generation tau tracers have failed to identify PSP-type 4R pathology in vivo due to off-target binding in typical 4R aggregation sites such as the pallidum and overall low affinity to 4R tau [13–16]. In contrast, the 2nd generation tau-PET tracer [18F]PI-2620 binds to PSP-type 4R and AD-type 3/4R tau in vitro [17– 19] and shows elevated [18F]PI-2620 PET binding in PSP in subcortical 4R predilection sites such as the pallidum and putamen [15, 20–24]. Further, autoradiography studies illustrated [18F]PI-2620 co-localization with 4R tau deposits in post-mortem PSP tissue [15, 20, 25], which we further confirmed by showing [18F]PI-2620 PET to autopsy correlations of tau severity in PSP patients [25]. Conclusively, these findings render [18F]PI-2620 a promising candidate to detect 4R tau in vivo in PSP [26-28]. Therefore, establishing [18F]PI-2620 as a 4R tau biomarker holds the potential to transform molecularly informed PSP diagnosis, to gain mechanistic insights into PSP pathophysiology, to benchmark other candidate 4R tau biomarkers and to track disease progression in clinical trials.

However, optimal quantification of [¹⁸F]PI-2620 PET remains challenging due to low to moderate increases in tracer uptake in typical 4R tau-vulnerable subcortical regions compared to the 3/4R tauopathy AD, where cortical tau-PET increases are much stronger [15, 29]. We argue that a potential key confound of [¹⁸F]PI-2620 PET quantification in 4R tauopathies like PSP is the choice of an optimal reference region used to scale the tau-PET signal in pathology harboring regions against an ideally pathology free region. The common standard for tau-PET assessment is intensity normalization to an inferior cerebellar grey matter (GM) reference, which has been developed for assessment of tau pathology in AD, where the cerebellum typically shows little

to no tau pathology [30, 31]. This is, however, problematic as post-mortem studies found that 4R tau accumulates in the cerebellar dentate nucleus and in oligodendrocytes in close vicinity to the cerebellar cortex in PSP, thereby potentially confounding PET quantification when using a cerebellar GM reference [24, 32, 33]. In addition, part of the cerebellar vermis and falx cerebri are typical off-target binding sites for [18F]PI-2620 due to binding to (neuro)melanin [34, 35]. Therefore, it is crucial to determine a more suitable reference region for optimal quantification of 4R tau, to enhance [18F]PI-2620 PET usage for assessing PSP in clinical and research settings. Hence, our major goal was to improve [18F]PI-2620 PET quantification in 4R tauopathies by identifying an optimized reference region for 4R tau, using a fully data-driven approach.

To this end, we used dynamic 0-60 min [18F]PI-2620 tau-PET from a discovery cohort of 58 PSP-RS patients and 18 healthy controls (HC). We quantified cerebral [¹⁸F] PI-2620 PET via an unbiased image-derived input function (IDIF) approach, using a pre-established automated extraction of carotid PET timeseries to calculate total volume of distribution (VT) images without the usage of a predefined tissue reference [36]. We have shown previously that carotid-based IDIF quantification of [18F]PI-2620 PET is strongly correlated to invasive arterial sampling, therefore offering a non-invasive alternative for reference region free quantification of cerebral PET tracer uptake [36]. IDIF-based VT images were iteratively referenced to atlas-based bilateral white-matter (WM) regions to identify an optimized PET reference region that allows optimal PSP-RS vs. HC group discrimination using the pallidum as a pre-established visual and quantitative 4R targeting readout [15, 37]. WM reference candidate regions leading to the strongest PSP vs. HC group differences were merged into one novel reference. This data-driven reference region was then applied to an independent validation cohort of PSP-nonRS (n = 54) and disease controls (AD =22, α -synuclein =21) to compute intensity-normalized IDIF-based VT ratios (VTr) as well as 20-40 min standard uptake value ratios (SUVr) for evaluating its' use in pre-established PSP-tailored static imaging protocols for [18F]PI-2620 PET [37, 38]. Using these data, we evaluated the novel data-driven WM reference region against the conventional inferior cerebellar GM reference by comparing mean SUVr's and VTr's derived from typical 4R (i.e., pallidum) and 3/4 accumulation sites (i.e. temporal meta region) between PSP, HC, AD and α-synuclein patients for cross-disease comparisons. Using receiver operating curve (ROC) analysis, we further determined the diagnostic performance of [18F]PI-2620 PET referenced to either temporo-orbital WM or inferior cerebellar GM and determined cut-off values for identifying PSP. Lastly, we



investigated whether higher pallidum [¹⁸F]PI-2620 PET predicted stronger PSP-associated functional deficits. An overview of our overall approach is depicted in Fig. 1.

Methods

Sample

We included 58 patients with PSP-RS as well as 54 PSP-nonRS patients as a validation sample. All PSP-RS and -nonRS patients were amyloid-biomarker negative based on routine CSF or amyloid-PET assessments to rule out concomitant AD pathology. The PSP-nonRS sample consisted

of individuals with CBS (n=41), PSP with predominant frontal presentation (PSP-F, n=6), predominant parkinsonism (PSP-P, n=4), predominant speech/language disorder (PSP-SL, n=1), predominant progressive gait freezing (PSP-PGF, n=1) and predominant primary lateral sclerosis (PSP-PLS, n=1). Further, we included 43 disease controls, i.e., 21 patients with α -synucleinopathies (α -syn) and 22 amyloid-biomarker positive (i.e., CSF or PET) patients across the AD spectrum. The α -syn sample consisted of individuals with dementia with Lewy bodies (DLB, n=4), Parkinson's disease (PD, n=13), Parkinson's disease with dementia (PDD, n=1) as well as multiple system atrophy of the cerebellar type (MSA-C, n=2) and Parkinsonian type (MSA-P, n=1) [7, 39, 40]. As a HC reference sample, we

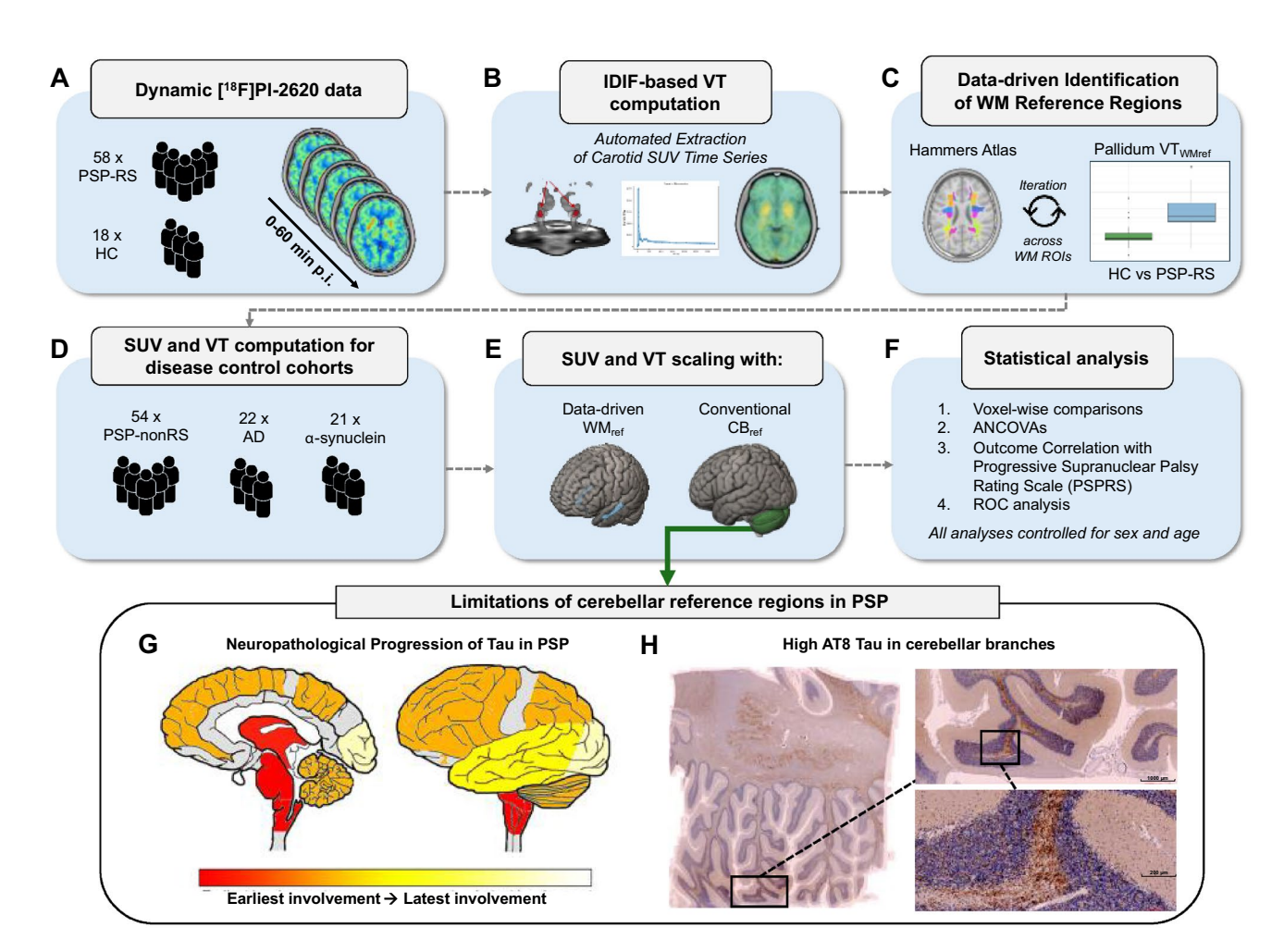


Fig. 1 Analysis flow chart. A Dynamic 0–60 min [18 F]PI-2620 PET data of 58 patients with PSP-RS and 18 HC were used to compute **B** IDIF-based VT images by an automated extraction method of carotid SUV timeseries. **C** Using a data-driven approach, 27 bilateral WM regions obtained from the Hammers Atlas were iteratively tested as potential candidates for intensity-normalization. Emerging WM regions leading to the largest group differences between PSP-RS patients and HC were combined into one new reference region spanning the temporo-orbital WM (WM_{ref}). **D** Using 20–40 min SUVr and VTr from PSP-RS, PSP-

nonRS, AD, α -synuclein and HC, **E** both references were compared by **F** voxel-wise comparisons, ANCOVAs, association with PSP rating scale and ROC analysis. Limitations of Cerebellar Reference Regions in PSP. **G** Neuropathological progression of tau in PSP as evidenced by Kovacs et al. showcasing that 4R tau is accumulating in oligodendrocytes that are located in WM branches in the vicinity to cerebellar GM in later disease stages [24]. **H** AT8 immunohistochemistry results of cerebellar PSP tissue showing the accumulation of tau in vicinity to GM



included 18 subjects without any evidence of neurological or psychiatric disorders. In a subset of PSP patients, we further employed the PSP rating scale (PSPRS) as a marker of PSP-typical clinical disease severity [41]. Written informed consent for PET-imaging was collected from all participants, and ethical approval was obtained by the institutional ethics committee at the University Hospital of Munich, LMU Munich, Germany (application numbers 17–569, 19–022).

Dynamic [18F]PI-2620 PET imaging

[18F]PI-2620 was synthesized as previously described [38]. PET imaging was performed at the Department of Nuclear Medicine at the LMU University Hospital in a full dynamic setting (0–60 min post-injection (p.i.)) using a Siemens Biograph True point 64 PET/CT or Siemens mCT (Siemens, Erlangen, Germany). The administered activity dose ranged between 156 and 218 MBq (median administered activity: 189 MBq) applied as a slow (10 s) intravenous bolus injection. The dynamic brain PET data was acquired in list-mode over 60 min and reconstructed into 35 time frames (12×5 s, $6 \times 10 \text{ s}$, $3 \times 20 \text{ s}$, $7 \times 60 \text{ s}$, $4 \times 300 \text{ s}$ and $3 \times 600 \text{ s}$) using a $336 \times 336 \times 109 \text{ matrix (voxel size: } 1.02 \times 1.02 \times 2.0 \text{ mm}3)$ and the built-in 3-dimensional ordered subset expectation maximization (OSEM) algorithm with 4 iterations, 21 subsets and a 5 mm full-width-at-half-maximum Gaussian filter on the Siemens Biograph and with 5 iterations, 24 subsets and a 5 mm full-width-at-half-maximum Gaussian filter on the Siemens mCT. A CT was used for attenuation correction (tube voltage: 120 kV, tube current: 33 mA, pitch: 1.5, rotation time: 0.5 s). As scatter correction, single scatter simulation was used.

Image processing and automated image derived input function modelling of dynamic [18F]PI-2620 PET data

VT images were computed using a previously established in-house dynamic PET pipeline, which computes an IDIF using an automated extraction of carotid artery SUV timeseries [36]. First, dynamic [¹⁸F]PI-2620 PET images were motion corrected via a stepwise co-registration using FSL, subsequently averaged into a mean 20–40 min PET image which was warped to the Montreal Neurology Institute (MNI) space via a 20–40 min [¹⁸F]PI-2620 custom in-house MNI summation template using the advanced normalization tools (ANTs) software. To compute IDIF, an independent component analysis (ICA) with a pre-defined 10 component solution was applied to the native space dynamic PET image, parcellating the image with the rationale that voxels belonging to the carotid artery show a highly temporally correlated SUV signal during early frames of the dynamic scan.

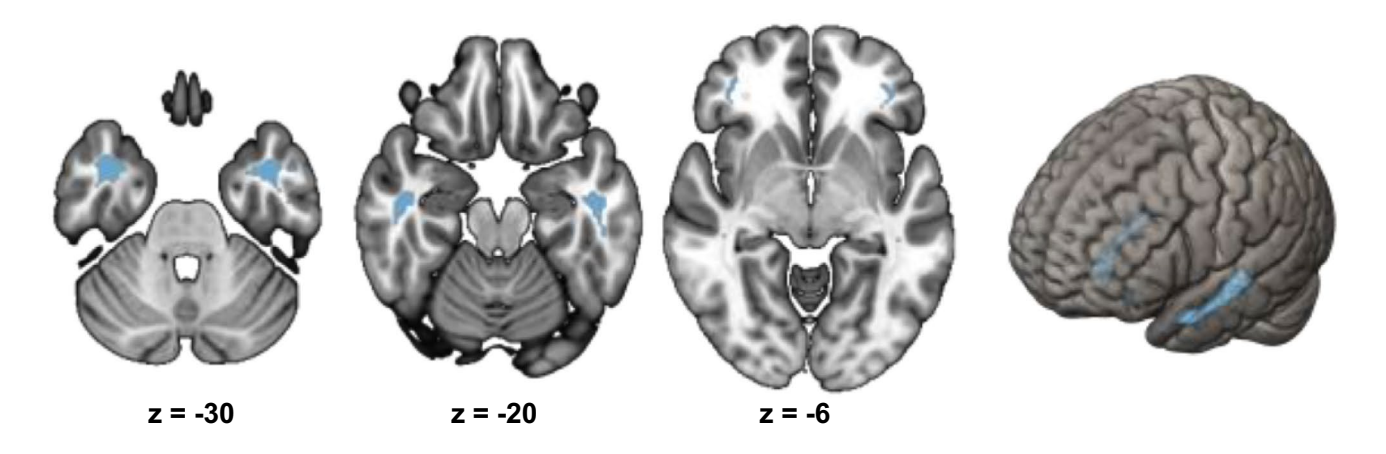
The resulting component maps were warped to MNI space using the prior obtained ANTs-derived high-dimensional warping parameters, spatially correlated with a custom in-house carotid artery template to select subject-specific carotid components maps and then masked using a binary image which restricts the carotid artery to a segment in the upper part of the pars cervicalis. Using the ANTs derived warping parameters, the masked subject-specific carotid image was warped back to PET native space with nearest-neighbor interpolation to preserve a binary image and further eroded using FSL to eliminate signal confounding voxels close to the vessel walls. Finally, the eroded binary carotid image was adjusted to the native space dynamic PET image to extract the SUV timeseries across the 60-minute [18F]PI-2620 PET scan [38]. IDIFs were generated by automated extraction of the maximum PET signal intensity from the carotid mask over the 60-minute dynamic PET scan, using our pre-established approach that closely resembles timeseries determined via an invasive arterial input function [36]. For quantification of [18F]PI-2620 PET binding differences, VT images were calculated using Logan plots [42] and spatially normalized to MNI space, using the ANTs derived normalization parameters.

Data-driven identification of a [¹⁸F]PI-2620 reference region for 4R tauopathies

Through an iterative approach, IDIF-based VT images were intensity-normalized (i.e. VTr) to 27 bilateral WM regions of the Hammers Brain Atlas [43] to identify reference regions where pallidum VTr values show the largest PSP-RS vs. HC group difference. The pallidum was selected as key readout as it resembles a typical 4R predilection site in both PSP-RS and PSP-nonRS as determined on postmortem and [18F]PI-2620 tau-PET data [4, 15, 24, 44]. All tested WM regions were first eroded using FSL and a 2 mm kernel to minimize potential spillover of confounding PET signal from adjacent grey matter structures [45]. Subcortical nuclear or cortical structures were excluded from the analyses as these regions have a higher likely-hood of specific or non-specific tau-tracer uptake and are thus not suitable as reference for intensity-normalization. Using those VTr images defined for each WM ROI of the Hammers atlas, we determined PSP-RS vs. HC group differences in pallidum VTr's, using ANCOVAs adjusted for age and sex. Subsequently, WM references surviving an FWE-based multiple comparison correction (p < 0.05) were combined into a single reference spanning the bilateral temporal and orbital WM (Fig. 2, Supp. Table 1). For subsequent in-depth comparison of this novel data-driven temporo-orbital WM reference vs. the conventional inferior cerebellar GM reference, we determined VTr and static 20–40-minute [¹⁸F]



Data-driven temporal-orbital WM reference region



Conventional inferior cerebellar reference region

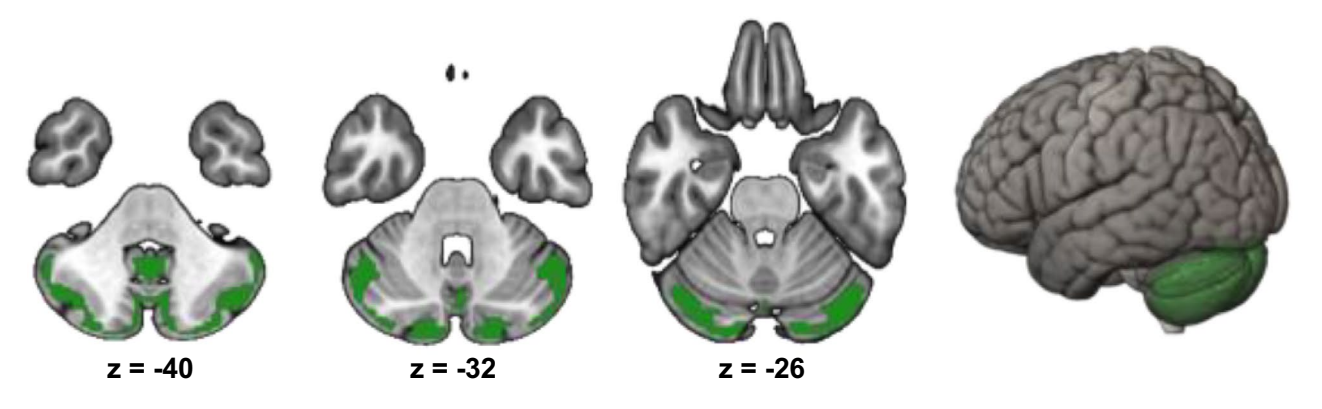


Fig. 2 Reference region visualization. Structural MRI slices and brain renderings were used to visualize temporo-orbital WM (first row) and inferior cerebellar GM (second row)

PI-2620 PET SUVRs for PSP-RS, PSP-nonRS (n = 54), disease controls (i.e., α -syn, n = 21; AD, n = 22) and HC (n = 18) adjusting to temporo-orbital WM and inferior cerebellar GM, respectively (Fig. 2, Supp. Figs. 1 and 2).

Statistics

MATLAB version R2023b (Statistical Parameter Mapping Software, The MathWorks Inc., Portola Valley, United States) and R Version 4.4.1 were used for statistical testing [46]. All analyses were conducted for intensity scaled VT (i.e. VTr) and SUV (i.e., SUVr) data, that were intensity normalized to a conventional inferior cerebellar GM or the data-driven temporo-orbital WM reference. To assess binding differences in SUVr and VTr PET data between PSP and disease samples with HC, a cluster-corrected voxel-wise comparison (voxel-level p< 0.001, cluster level $p_{\rm FWE}$ <0.05) was conducted using SPM12 (Wellcome Trust Centre for

Neuroimaging, University College London), adjusting for age and sex. Further, a ROC analysis was performed to estimate the optimal [18F]PI-2620 SUVr and VTr thresholds for discrimination of PSP-RS and PSP-nonRS groups from HC. Areas under the curve (AUC) for both reference regions were compared using a non-parametric approach as previously described [47]. For targeted across-disease group assessments, analysis of covariance (ANCOVA) adjusted for age and sex was employed to test for differences between average [18F]PI-2620 SUVr and VTr values in the pallidum and the AD-tailored temporal meta ROI [48] between all cohorts. Pairwise comparisons were conducted to correct for multiple testing using the Tukey adjustment, and effect sizes (Cohen's d) were calculated for between group comparisons. To evaluate associations between mean SUVr and VTr pallidum scores and the PSPRS as a measure of clinical disease severity, linear regression models adjusted for age and sex were applied. P values less than



0.05 were considered significant (* p< 0.05, ** p< 0.01, *** p< 0.001).

Results

Sample description

Sample demographics and clinical characteristics are shown in Table 1. Overall, we included 58 PSP-RS patients (35 men [60.3%]; mean [SD] age, 70.6 [7.9] years; mean [SD] PSPRS score, 34.1 [9.2]) and 54 PSP-nonRS patients (30 men [55.6%]; mean [SD] age, 71.7 [6.3] years; mean [SD] PSPRS score, 29.1 [14.0]). PSPRS scores capturing clinical disease severity were available for a subset of patients (PSP-RS = 40, PSP-nonRS = 40) and did not differ between PSP-RS and non-RS (p= 0.06). In addition, we included 22 AD patients (12 men [54.5%]; mean [SD] age, 73.8 [9.8] years) and 21 α -syn patients (15 men [71.4%]; mean [SD] age, 63.0 [10.5] years) as disease controls as well as 18 HC (9 men [50%]; mean [SD] age, 71.7 [8.4] years). There was a significant difference in age between groups, where α -syn patients were younger than PSP and AD groups (p< 0.05).

Validation of the data-driven temporo-orbital WM reference for assessment of 4R tauopathies

When applying the data-driven temporo-orbital WM reference to the PSP-RS sample and the independent PSP-nonRS cohort (n=54) for intensity normalization, voxel-wise comparisons (p < 0.001, FWE-cluster corrected at p < 0.05) yielded strong group differences in 20–40 min SUVrs for PSP-RS vs. HC and similarly for PSP-nonRS vs. HC (Fig. 3). When applying the temporo-orbital WM reference to the disease controls, we detected cortical temporo-parietal SUVr increases in AD vs. HC, while only minor group differences were detected for α -syn vs. HC groups in meningeal regions, confirming the specificity of the temporo-orbital WM reference region as per tau positive (i.e. AD) and negative (i.e., α -syn) disease controls. To contrast these analyses against conventional PET quantification approaches, the

widely used inferior cerebellar GM reference was used to calculate SUVr with the same 20–40-minute [18 F]PI-2620 PET data for all samples. Using voxel-wise comparisons (voxel-level p< 0.001, FWE-cluster corrected at p< 0.05), only minimal group differences in the basal ganglia SUVr values were detected for PSP–nonRS vs. HC and PSP-RS vs. HC (Fig. 3). Usage of VTr's instead of static SUVr's yielded overall congruent results (Supp. Figure 3).

We further ran ROC analyses to determine AUCs and [¹⁸F]PI-2620 PET cut-offs for separating PSP-RS and PSPnonRS from HC groups using the PET SUVr's or VTr's of significant clusters in the basal ganglia displayed in Fig. 3. AUCs were compared between SUVr or VTr data scaled to either the temporo-orbital WM or the inferior cerebellar GM reference. For SUVr data within the basal ganglia clusters we found an AUC of 0.92 for PSP-RS vs. HC when using the temporo-orbital WM reference, which was significantly (p < 0.015) better than the AUC of 0.82 obtained when using the inferior cerebellar GM reference (Fig. 4A). Congruent results were obtained for PSP-nonRS vs. HC, with AUCs of 0.94 vs. 0.78 (p < 0.0003) Fig. 4B) for temporo-orbital WM referenced vs. inferior cerebellar GM referenced SUVr's or when using VTr's instead of SUVr's (Fig. 4C, D). Sensitivities and specificities as well as ROC-based cut-point for PSP vs. HC stratified by reference region are shown in Table 2. As sensitivity analysis, we recomputed the ROC analysis using atlas-based SUVr and VTr pallidum PET values and found congruent results (Supp. Figure 4). Overall, these findings suggest that the data-driven temporo-orbital WM reference improves the potential of [18F]PI-2620 PET to assess 4R tau pathology in PSP patients.

Targeted assessment of [¹⁸F]PI-2620 for quantification of 4R pallidum Tau and AD-type cortical Tau deposits

In a next step, we performed a targeted ROI-based analysis of [18F]PI-2620 to further illustrate [18F]PI-2620 PET signal differences between PSP vs. HC and disease controls, when specifically assessing the pallidum as a key 4R target region. In addition, we also included the temporal meta ROI as a

Table 1 Sample characteristics

Variable	PSP-RS (n = 58)	PSP–nonRS ($n = 54$)	AD $(n = 22)$	α -syn ($n = 21$)	HC (n = 18)	P
Subgroups	PSP-RS	PSP-CBS $(n = 41)$	NA	PD $(n = 13)$	NA	'
		PSP-F $(n = 6)$		DLB $(n = 4)$		
		PSP-P (n = 4)		PDD $(n = 1)$		
		PSP-SL(n=2)		MSA-C (n = 2)		
		PSP-PLS (n = 1)		MSA-P(n=1)		
Age	70.6 ± 7.9	71.7±6.3	73.8 ± 9.8	63.0±10.5	71.7 ± 8.4	0.0001
Sex (m/f)	35/23	30/24	12/10	15/6	9/9	0.664
PSPRS*	34.1 ± 9.2	29.1±14.0	NA	NA	NA	0.0618

Age and PSPRS values are presented as mean±SD. *PSPRS scores were available for a subset of 40 PSP-RS patients and 40 PSP-nonRS patients



Voxel-wise SUVr comparisons: disease vs controls (FWE-corrected, p<0.001)

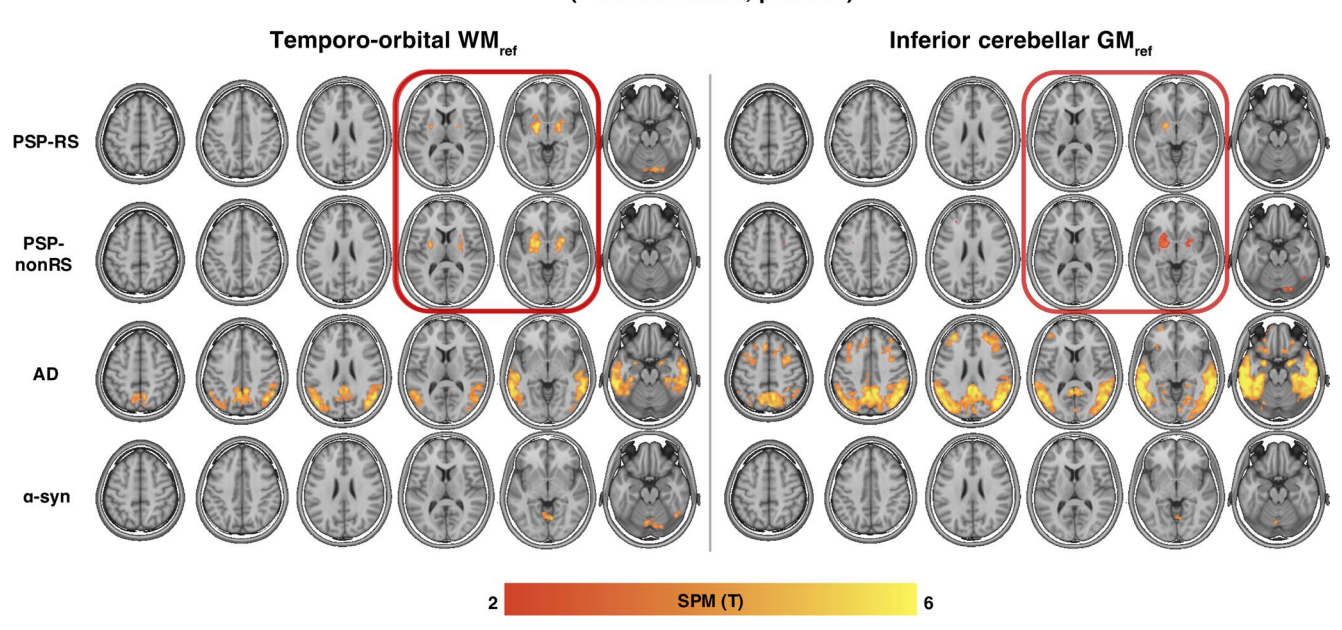


Fig. 3 Voxel-wise Group Comparison between Disease Samples (PSP-RS, PSP-nonRS, AD, α-syn) and HC. Comparisons were conducted by utilizing 20–40 minute [18 F]PI-2620 SUVr PET intensity-normalized with temporo-orbital WM (WM_{ref}) or conventional inferior cerebellar

GM (GM_{ref}). Models were adjusted for sex and age and P values corrected via cluster correction (voxel p < 0.001, FWE-cluster correction, p < 0.05). Yellow voxels indicate stronger group differences

AD-typical target region for 3/4R tau [48]. Pallidum and a temporal meta ROI SUVrs were compared across all disease samples and HC using either the temporo-orbital WM reference or the inferior cerebellar GM reference. Group comparisons of SUVr normalized with temporo-orbital WM revealed significantly elevated [18F]PI-2620 binding in the pallidum in patients with PSP-RS and PSP-nonRS compared to HC and disease controls (α-syn and AD) (Fig. 5A). In addition, AD patients showed slightly elevated yet significant binding differences in the globus pallidus compared to HC and α-syn. When using the conventional inferior cerebellar GM reference, we found lower, yet significant group differences in pallidum SUVr's for PSP-RS vs. HC and disease controls, between PSP-nonRS and α-syn patients (Fig. 5B). However, there was no group difference between PSP-nonRS vs. HC and AD patients. Standardized effect sizes of these group comparisons are shown in Fig. 5C; Table 3, illustrating overall large group differences in PSP patients vs. HC and disease controls when using the temporo-orbital WM reference instead of the inferior cerebellar GM reference.

For a targeted readout of AD-type 3/4R tau, we ran the same analyses using the AD-tailored temporal meta ROI, showing consistent group differences between AD patients and PSP, HC and α-syn patients when using the temporo-orbital WM reference (Fig. 5D) or the inferior cerebellar GM reference (Fig. 5E), yet standardized group differences

were overall larger for AD patients vs. HC and disease controls when using the inferior cerebellar GM reference (Fig. 5F). Together, these results suggest that the data-driven temporo-orbital WM reference provides superior performance for the assessment of PSP, while the conventional inferior cerebellar GM reference provides superior performance for the assessment of AD. Group comparisons of VTr values revealed similar results, with elevated [¹⁸F]PI-2620 binding in the globus pallidus observed in patients with PSP-RS and PSP-nonRS compared to HC and disease controls (Supp. Figure 5).

[¹⁸F]PI-2620 PET referenced to temporo-orbital WM reference is associated with clinical PSP severity

Lastly, we determined whether [18 F]PI-2620 PET quantification using the novel data-driven temporo-orbital WM allows tracking clinical disease severity. To this end, we determined the association between pallidum PET signal as a key 4R target regions and the PSPRS score, using linear regression controlling for age and sex. Since PSPRS scores were only available for a subset (i.e., PSP-RS, n= 40; PSP-nonRS, n= 40), we merged both PSP-RS and PSP-nonRS groups for this analysis to maximize statistical power. We found significant associations between higher pallidum [18 F] PI-2620 PET and higher PSPRS scores when using SUVr (β = 0.34, p< 0.001, Fig. 6A) scaled to the temporo-orbital



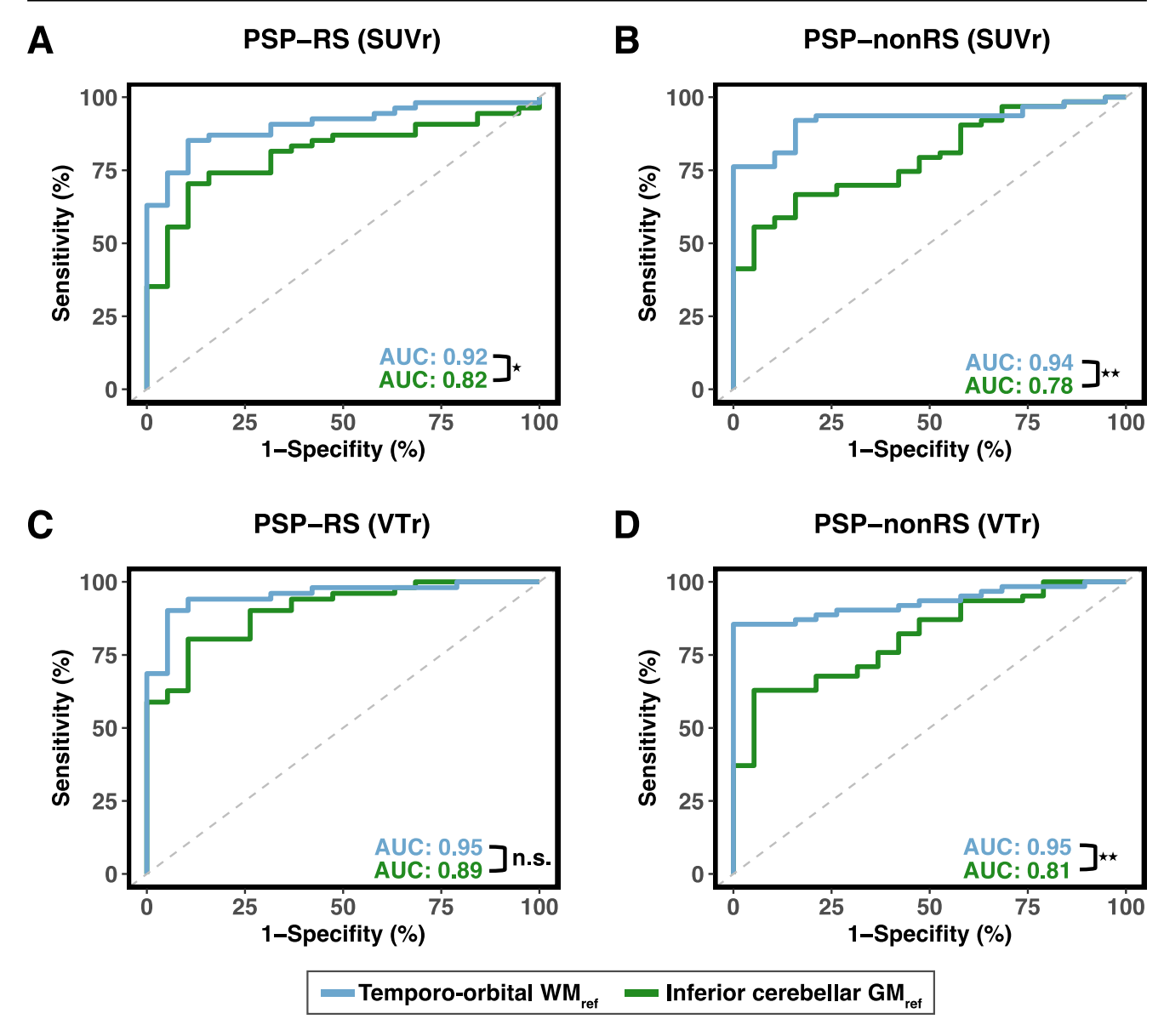


Fig. 4 Definition of [¹⁸F]PI-2620 PET Cut-offs for Identifying PSP Patients. ROC curves were compared in their discriminative power between [¹⁸F]PI-2620 SUVr data (A, B) scaled either with tempororbital WM (blue line) or inferior cerebellar GM (green line) as reference for PSP-RS vs. HC (**A**, **C**) and PSP-nonRS vs. HC (**B**, **D**). SUVr

and VTr cut-off calculation was performed and computed for both PSP samples. ROC curves were compared using a non-parametric approach as previously established by DeLong and colleagues [47]. Asterisks are used to illustrate level of significance *** = p< 0.001, ** = p< 0.05. Results are reported in the text

Table 2 Sensitivity, specificity and cut-offs for pallidum [18F]PI-2620 PET for PSP vs. HC comparisons

Cohort	Parameter	Reference	Sensitivity	Specificity	AUC	Cut-Off
PSP-RS	SUVr	Temporo-orbital WM	0.86	0.89	0.92	1.07
	SUVr	Inferior Cerebellum GM	0.76	0.83	0.82	1.44
	VTr	Temporo-orbital WM	0.85	0.94	0.95	1.18
	VTr	Inferior Cerebellum GM	0.78	0.89	0.89	1.07
PSP-nonRS	SUVr	Temporo-orbital WM	0.94	0.83	0.94	1.09
	SUVr	Inferior Cerebellum GM	0.69	0.83	0.78	1.40
	VTr	Temporo-orbital WM	0.91	0.94	0.95	1.17
	VTr	Inferior Cerebellum GM	0.64	0.94	0.81	1.23



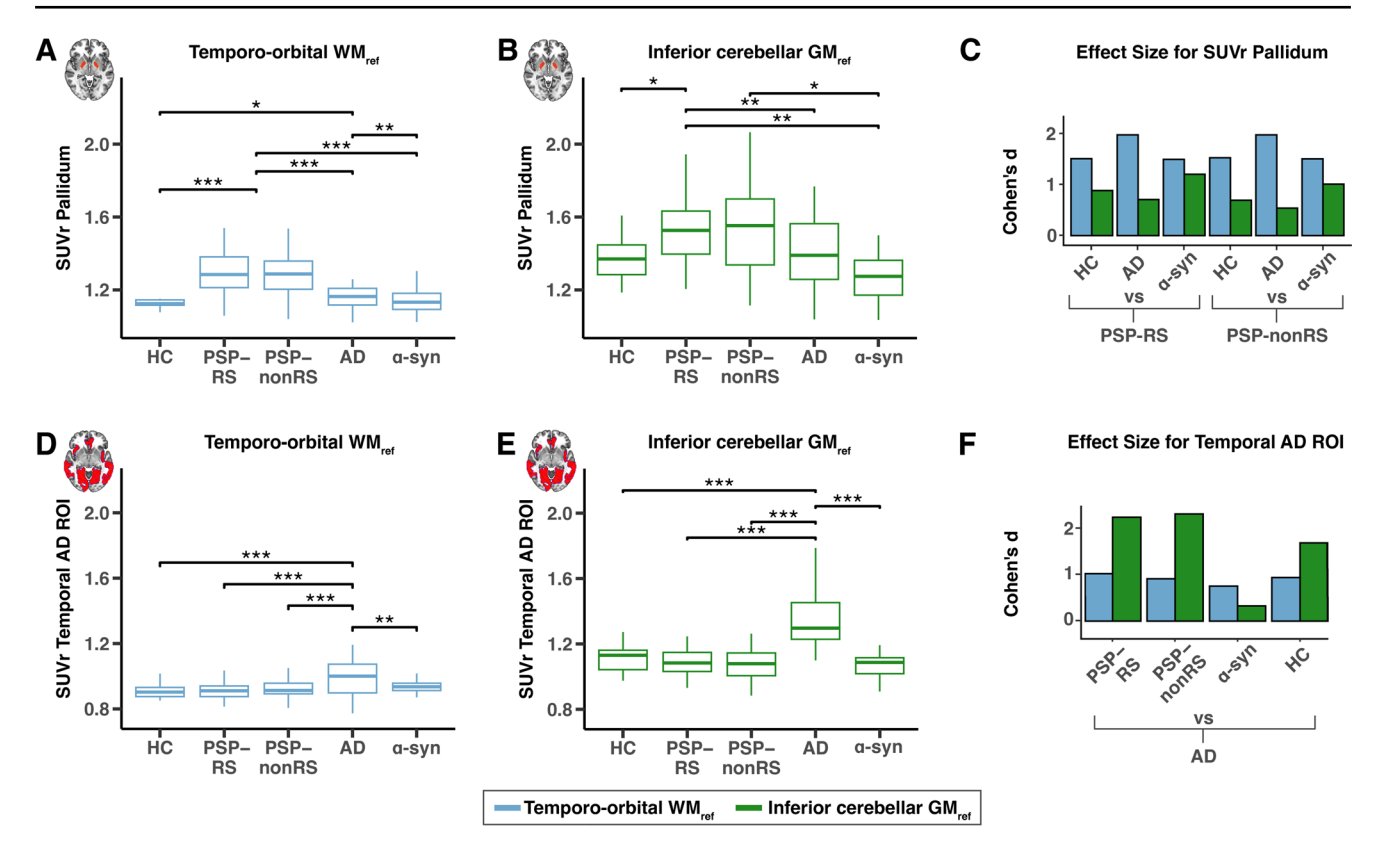


Fig. 5 Results of ANCOVA computed for average SUVr pallidum values ($\bf A, B$) and average SUVr values derived from a temporal AD signature ROI ($\bf D, E$). Boxplots illustrating mean 20–40 min [18 F]PI-2620 PET SUVr data for each cohort. SUVr data were either intensity-normalized via a temporo-orbital WM_{ref} ($\bf A, D$) or with conventional

Table 3 Effect sizes of [¹⁸F]PI-2620 PET pallidum SUVr differences in PSP vs. HC and disease controls stratified by reference region

Disease group	Group comparison	Temporo-	Inferior	
		orbital WM	Cere- bellum	
			GM	
PSP-RS	Cohen's d (vs. HC)	1.48	0.68	
	Cohen's d (vs. AD)	1.94	0.53	
	Cohen's d (vs. α-syn)	1.47	0.99	
PSP-nonRS	Cohen's d (vs. HC)	0.87	1.50	
	Cohen's d (vs. AD)	0.70	1.94	
	Cohen's d (vs. α-syn)	1.18	1.48	

WM. In contrast, no such association was found when scaling SUVr's to the inferior cerebellar GM reference (β = 0.03, p= 0.8, Fig. 6B). Congruent results were obtained for VTr's, showing an association with PSPRS scores when scaled to the temporo-orbital WM (β = 0.24, p= 0.03, Fig. 6C) vs. the inferior cerebellar GM (β = 0.02, p= 0.88, Fig. 6D). Results were congruent when tested separately for PSP-RS and PSP-nonRS cohorts (Supp. Figs. 6 and 7). Therefore, these results suggest that higher [18 F]PI-2620 PET signal in the pallidum as a key 4R target region is related to stronger

inferior $GM_{ref}(\mathbf{B}, \mathbf{E})$. Barplots illustrate effect size with Cohen's d for PSP cohorts vs. (C) and AD vs. control cohorts (F). Asterisks are used to illustrate level of significance *** = p < 0.001, ** = p < 0.05. Blue: Temporo-orbital WM. Green: Inferior cerebellar GM

clinical impairment, when using the novel data-driven temporo-orbital WM reference.

Discussion

The main aim of this study was to optimize [18F]PI-2620 assessment as a 4R tau biomarker in PSP by addressing key limitations of the commonly used inferior cerebellar GM tau-PET reference [49], which is potentially confounded by adjacent cerebellar 4R tau accumulation [24, 33]. To address this, we obtained 60 min full dynamic [18F]PI-2620 PET data from PSP-RS patients (n = 58) and HC (n = 18), and computed IDIF-based VT images via referencing to carotid blood PET timeseries as a proxy of arterial tracer concentrations that are unbiased by 4R tau and corrected for differences in blood flow [36]. Using these VT images, we employed a data-driven approach to identify an optimized [18F]PI-2620 reference region for PSP assessment. Specifically, we performed iterative PET-intensity normalization of IDIF-derived VT images across atlas-based bilateral WM regions, based on which we benchmarked PSP-RS vs.



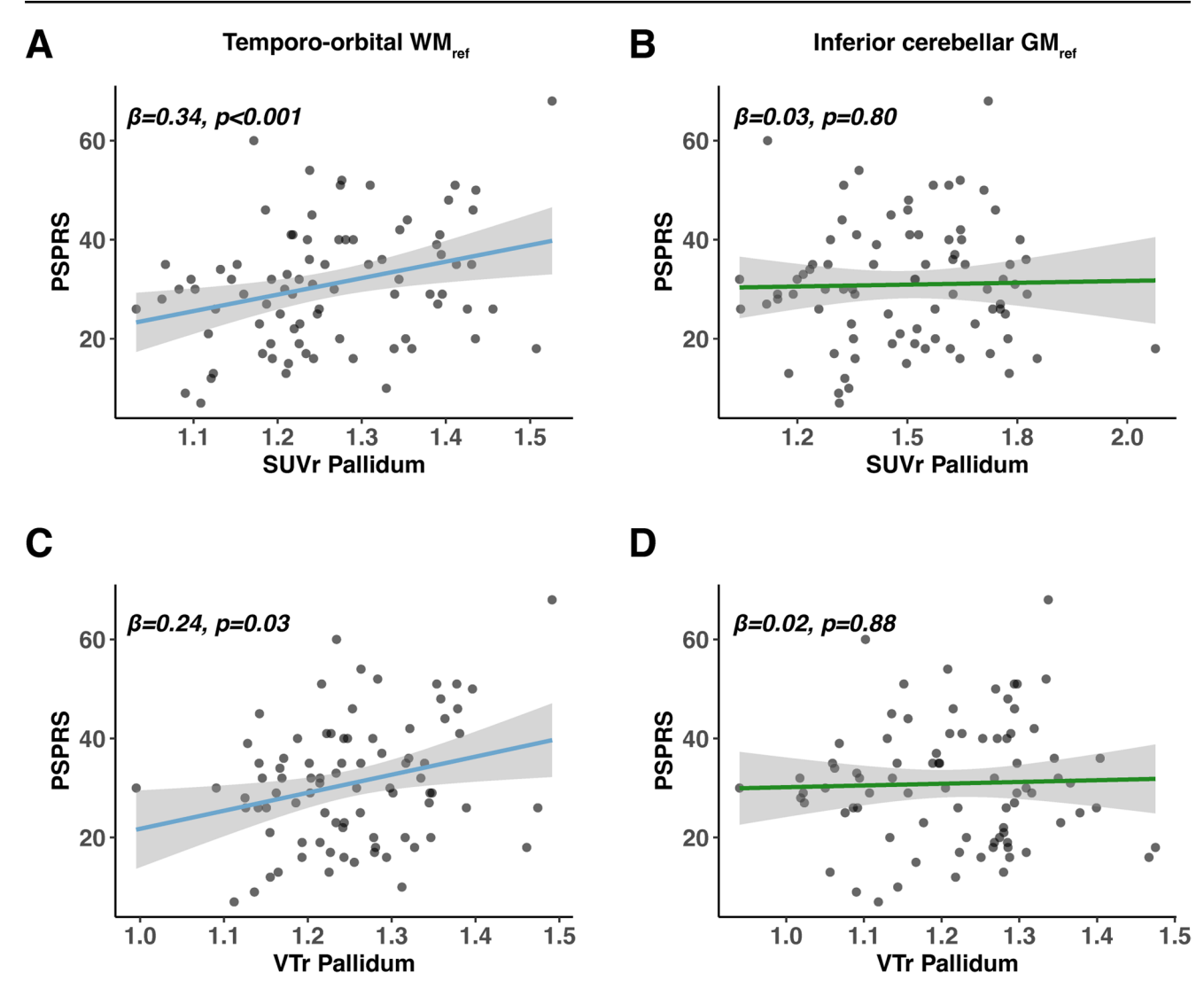


Fig. 6 Results of Linear Regression Analyses. Scatterplots illustrating the association between mean 20–40 min [¹⁸F]PI-2620 PET SUVr and VTr data from the pallidum with disease severity (PSP rating scale).

SUVr and VTr images were either referenced with temporo-orbital WM (A, C) or conventional inferior cerebellar GM (B, D)

HC group-separation using the pallidum as a 4R tau target region, adjusting for age and sex [15]. The best performing WM candidate regions surviving multiple comparison correction were then combined into a single temporo-orbital WM reference, which maximized PSP-RS vs. HC group differences in the pallidum. This data-driven temporo-orbital WM reference was then used for [18F]PI-2620 PET quantification in an independent validation cohort of PSP-nonRS patients (n = 54) and non-4R disease controls including AD (n=22) and α -synucleinopathies (n=21). Compared to using the conventional inferior cerebellar GM tau-PET reference [49], we found that referencing [18F]PI-2620 to the novel temporo-orbital WM reference yielded (i) stronger bilateral basal ganglia tau-PET signal in PSP vs. HC, (ii) larger group differences between PSP vs. disease controls in 4R target regions, and (iii) significant associations of pallidum [18F] PI-2620 PET signal with clinical disease severity. All results were consistent for intensity normalized VTr's as well as static 20–40 min SUVr's, suggesting that the novel temporo-orbital WM reference can be applied to static [¹⁸F]PI-2620 in PSP, thereby facilitating its' clinical implementation via shorter 4R-tailored 20–40 min static imaging protocols [37, 38]. Together, our results suggest that a data-driven temporo-orbital WM reference for intensity scaling of [¹⁸F]PI-2620 PET outperforms the conventional inferior cerebellar GM reference for assessing 4R tau in PSP.

A major strength of our study is the use of non-invasively derived, reference-region-free, IDIF-based VT images for quantification of [¹⁸F]PI-2620 tau-PET [36]. Unlike other non-invasive PET quantification methods, this approach does not require the a priori selection of a reference tissue, which may potentially harbor 4R tau and thus bias the subsequent



identification of an optimized reference region for PSP [50]. Importantly, our pre-established approach for assessing of carotid [18F]PI-2620 timeseries is fully automated, which further minimizes manual user input and bias [36]. We have previously shown that our fully-automated assessment of carotid [18F]PI-2620 PET timeseries aligns closely with invasive arterial input functions in PSP, thereby supporting its validity to derive robust and unbiased estimates of cerebral [18F]PI-2620 PET binding [36]. As candidate reference regions, we focused particularly on WM regions due to the following rationale: We found previously using in vivo PET imaging and post-mortem autoradiography, that [¹⁸F] PI-2620 captures neuronal 4R tau in GM regions, as well as oligodendroglial tau at the GM/WM boundary [25]. However, we also reported that [18F]PI-2620 binding and AT8 stained tau pathology drops significantly when moving away from the GM/WM boundary towards the deeper WM [25]. Therefore, we specifically eroded the atlas-based WM candidate regions, to ensure sufficient distance of WM regions from the GM/WM boundary to avoid including tau harboring tissue in our reference. In an alternative approach, a previous study involving members of our study group employed [18F] PI-2620 intensity normalization using the fusiform gyrus GM and cerebellar crus as a reference, yielding improved PSP vs. HC separation [51]. Of note, the fusiform gyrus is right adjacent to our suggested temporo-orbital WM reference, suggesting that the temporal lobe may in general be suitable as a 4R reference region and harbor little 4R tau as partly supported by previous post-mortem evidence in PSP [24]. However, we also argue that using cortical GM tissue as a reference may be potentially biased in PSP cases with concomitant 3/4R AD-type tau pathology, which typically targets the fusiform gyrus in early disease stages [52, 53]. This is particularly relevant, since we found previously that AD co-pathology can be found in up to 84% of patients, with ~10% of patients showing Braak stage III tau pathology [54], which includes the fusiform gyrus [31, 54]. Thus, we propose that the temporo-orbital WM reference may more robust than a fusiform GM reference for [18F]PI-2620 assessment in PSP patients with and without AD co-pathology. However, this remains to be specifically tested in PSP cases with biomarker confirmed AD co-pathology.

Overall, our results on group differences in PSP patients vs. HC align well with previous PET and autopsy studies showing that the basal ganglia resemble a key 4R tau accumulation site that are likely reflected in [¹⁸F]PI-2620 signal increases in PSP patients [15, 44]. Supporting the validity of [¹⁸F]PI-2620 to bind to 4R tau, we have shown consistently that [¹⁸F]PI-2620 binds to 4R tau in vitro [20], that [¹⁸F]PI-2620 autoradiography colocalizes with AT8 tau stainings in postmortem PSP tissue [15, 20], and that the ante-mortem [¹⁸F]PI-2620 signal in the pallidum is associated with post-mortem

assessed AT8 tau staining intensity and [18F]PI-2620 autoradiography [25]. Of note, the current study emphasizes that [18F]PI-2620 signal increases in PSP vs. HC become larger when using the data-driven temporo-orbital WM reference compared to the conventional cerebellar reference [15, 20, 28, 55] that may be confounded by 4R tau pathology [15, 20, 24, 28, 55]. Importantly, these results generalized fully to an independent PSP-nonRS cohort which was not involved in the data-driven identification of the temporo-orbital WM reference. Our ROC analyses further supported the superiority of the temporo-orbital WM vs. inferior cerebellar GM reference, showing increased AUCs for detecting PSP patients vs. controls, providing preliminary VTr and SUVr cut-offs for determining [18F]PI-2620 abnormality in clinical and research settings. Of note, the AUC increases were more pronounced in PSP-nonRS phenotypes, in some of which the cerebellum has been suggested to accumulate 4R tau earlier than in patients with a PSP-RS phenotype [24]. This suggests that employing a temporo-orbital WM reference may improve [18F]PI-2620-based 4R tau assessments across different clinical PSP phenotypes. Yet, this remains to be tested systematically in future studies including larger numbers of different PSP-RS and PSP-nonRS phenotypes.

When further comparing [18F]PI-2620 PET signal intensities between PSP patients and disease controls, we found that usage of the temporo-orbital WM reference clearly improved group separation of PSP-RS and -nonRS groups vs. disease controls compared to using the conventional inferior cerebellar reference. These findings align with previous studies reporting only weak group differences between 4R tauopathies and disease controls in typical PSP regions such as the basal ganglia when using conventional cerebellar referencing approaches [15, 20, 28, 56, 57]. We argue, that this overall stronger [18F]PI-2620 PET signal increase in PSP vs. HC and disease controls using the temporo-orbital reference may stem from minimizing the influence of cerebellar 4R tau which may compromise 4R tau assessments when adjusting to the cerebellum, especially in advanced PSP cases [24]. Importantly, however, though the pallidum resembles a key 4R tau aggregation site [15, 20], a recent post-mortem study has shown that 65% of AD patients show AT8 positive tau deposits the basal ganglia, which may compromise PSP vs. AD comparisons [58]. Supporting this, we also observed significant basal ganglia tau-PET signal elevations in AD vs. HC and α-syn patients using the temporo-orbital WM reference. However, PSP patients showed much stronger [18F]PI-2620 PET increases in the pallidum, while AD exhibited greater cortical signal elevations (i.e., in the temporal meta ROI) than PSP groups. This supports our previously suggested workflows, that simultaneous assessment of both cortical and basal ganglia [18F]PI-2620 PET can aid in the biomarker-based differentiation of PSP vs. AD



[57]. In addition, [18 F]PI-2620 PET signals in tau vulnerable regions in AD patients are generally higher than in patients with 4R tauopathies which can be attributed to a stronger binding of [18 F]PI-2620 to AD-type 3/4R tau and a faster clearance for [18 F]PI-2620 tracer in 4R tauopathies [23]. Therefore, we have previously specifically suggested 20–40 min imaging windows for assessing PSP, which capture the early and transient increases of [18 F]PI-2620 binding to 4R tau in PSP [38]. Together, our results suggest that our novel reference region can improve the detection of PSP patients vs. HC and disease controls with overlapping clinical phenotypes (i.e. α -syn) using both dynamic scanning as well as shortened clinically feasible 20–40 min static imaging windows, thereby supporting its use as a biomarker for 4R tauopathies in clinical and research settings.

Importantly, we also detected a significant association between [18F]PI-2620 pallidum PET signal with clinical disease severity (i.e., PSP-RS) exclusively when using the temporo-orbital WM as a reference. This is a clear and major step forward for the clinical utility of [18F]PI-2620 in PSP, since we have previously failed to establish a clear and consistent association between [18F]PI-2620 PET and clinical disease severity [15, 55, 59]. In view of the current findings, we argue that a main confounder for assessing a link between PET signal intensity and clinical disease severity may lie in the choice of reference region. As mentioned above, cerebellar 4R tau accumulates predominantly in advanced PSP disease stages, thereby lowering the ratio of basal ganglia to inferior cerebellum PET signal in patients with more advanced clinical disease severity [24]. Hence, intensity normalization to a 4R tau harboring cerebellar reference can reduce PET signals in a 4R tau target site to a stronger degree in advanced PSP cases or rare PSP phenotypes with predominant cerebellar 4R accumulation [24]. Therefore, artificial lowering [18F]PI-2620 PET by a confounded reference in clinically advanced cases may mask a linear association of [18F]PI-2620 PET-assessed 4R tau levels with clinical scores across the PSP spectrum. This is also problematic for longitudinal studies, as it may clearly limit the opportunity to track 4R tau progression in cases where 4R tau accumulates in the cerebellum during follow up [24]. Here, our novel temporo-orbital reference may improve the detection of longitudinal [18F]PI-2620 PET increases, by referencing to a potentially pathology free region. We will specifically address this question in longitudinal studies, once sufficient data become available. Together, our results show that [18F]PI-2620 can track clinical disease severity in PSP and may therefore be suitable as a surrogate biomarker in disease modifying treatment.

When interpreting the results of our study, several limitations should be considered. First, for our data-driven approach we used a discovery cohort of PSP-RS patients and

validated our results in an independent validation cohort of PSP-nonRS patients. This might be problematic as regional tau distribution may drive clinical heterogeneity in PSP, which is not detected in the current group-level analyses [24]. However, results of our voxel-wise comparisons suggested that both PSP-RS and PSP-nonRS consistently show abnormal [18F]PI-2620 PET levels in the basal ganglia when compared to HC and disease controls. The strong increase in sensitivity for PSP-nonRS further establishes the validity of the pallidum as a key 4R readout for both PSP-RS and nonRS phenotypes. Second, due to missing structural MRI data, we did not perform partial volume correction which might lead to spill-over effects from grey matter regions [45]. This may be particularly relevant for applying our temporo-orbital WM reference in AD cases, where we saw less pronounced group separation between AD vs. HC, suggesting that spill in of cortical temporal lobe tau-PET signal to the temporo-orbital reference. Thus, in clinical settings, we would clearly recommend using inferior cerebellar GM and temporo-orbital WM references simultenously for caseto-case assessments. We tried to address potential partial volume effects and spill-over from the GM to WM regions by eroding all candidate WM reference ROIs by a 2 mm gaussian kernel to move away from grey matter. Yet, future studies should assess whether partial volume correction can further improve [18F]PI-2620 PET quantification in PSP and AD. Third, PSP was diagnosed purely using clinical criteria without autopsy confirmation, hence misdiagnoses may confound our overall results. Therefore, we are currently collecting autopsy data from patients with an antemortem [18F]PI-2620 PET scan, to further investigate the sensitivity and specificity of [18F]PI-2620 PET for assessing 4R tau using a gold-standard post-mortem diagnosis of 4R tau. Fourth, we used an IDIF-based method to compute VT images which is only an estimate of arterial sampling [36]. While an arterial-input function based approach might be more reliable, we could previously show that IDIF-based VTs are highly correlated with arterial-input-function-based VTs and thus eligible for quantification of [18F]PI-2620 PET [36].

In conclusion, our findings show that [18F]PI-2620 PET data scaled with temporo-orbital WM is superior to conventional reference region methods for quantification of tau in 4R tauopathies and could be used in clinical trials to track disease progression or aid in molecularly defined diagnosis of PSP. We argue, these results do not only indicate a greater clinical utility of temporo-orbital reference regions in applications for differential diagnosis of patients with suspected 4R tauopathies but may also facilitate the discovery of novel PSP biomarkers (e.g. fluid) using [18F]PI-2620 PET imaging as an established 4R tau quantification method. Our results should act as a starting point for additional studies to focus



on autopsy validation and longitudinal imaging to confirm and extend our findings and establish tau-PET imaging for PSP in the clinical setting.

Supplementary Information The online version contains supplementary material available at https://doi.org/10.1007/s00259-025-07396-8.

Author contributions Prof. Brendel had full access to all of the data in the study and takes responsibility for the integrity of the data and the accuracy of the data analysis. Concept and design: Frontzkowski, Franzmeier, Gnörich, Brendel. Acquisition, analysis, or interpretation of data: Katzdobler, Gnörich, Palleis, Gross, Frontzkowski, Franzmeier, Brendel. Critical revision of the manuscript for important intellectual content: Gnörich, Dehsarvi, Roemer-Cassiano, Dewenter, Steward, Biel, Hirsch, Zhu, Levin, Stephens, Müller, Koglin, Bischof, Kovacs, Höglinger, Franzmeier, Brendel. Drafting the manuscript: Frontzkowski, Franzmeier, Gnörich, Brendel. Statistical analysis: Frontzkowski, Gross, Gnörich, Franzmeier, Brendel. Supervision: Franzmeier, Brendel, Höglinger.

Funding Open Access funding enabled and organized by Projekt DEAL.

JG is funded by the Munich Clinician Scientist Program (MCSP). MB has received research support from Deutsche Forschungsgemeinschaft (EXC 2145 SyNergy– ID 390857198). This work was supported by a grant from the German Parkinson Society (DPG) awarded to NF.

Data availability All data are available from the corresponding author upon reasonable request and upon successful conclusion of a data transfer agreement with the principal investigators at the LMU hospital. The temporo-orbital WM reference can be found on GitHub (https://github.com/Franzmeierlab).

Declarations

Conflict of interest MB received speaker honoraria from GE health-care, Roche, and LMI and is an advisor of LMI. A.W.S., A.M., N.K. and G.N.B. are employed by LMI. G.H. received research support from GE Healthcare and Neuropore; has ongoing research collaborations with Orion and Prothena; serves as a consultant for AbbVie, Alz-Protect, Asceneuron, Biogen, Biohaven, Lundbeck, Novartis, Roche, Sanofi, UCB; received honoraria for scientific presentations from AbbVie, Biogen, Roche, Teva, UCB, and Zambon; and holds a patent on PERK Activation for the Treatment of Neurodegenerative Diseases (PCT/EP2015/068734). No other potential conflict of interest relevant to this article was reported.

Ethical approval All procedures performed in studies involving human participants were in accordance with the ethical standards of the institutional and/or national research committee (LMU Munich—application number 17–569) and with the 1964 Helsinki declaration and its later amendments or comparable ethical standards.

Informed consent Informed consent was obtained from all patients. All patients provided informed written consent to PET imaging. The study was conducted in accordance with the principles of the Declaration of Helsinki, and approval for scientific data analysis was obtained from the local ethics committee (application number 17–569).

Open Access This article is licensed under a Creative Commons Attribution 4.0 International License, which permits use, sharing, adaptation, distribution and reproduction in any medium or format,

as long as you give appropriate credit to the original author(s) and the source, provide a link to the Creative Commons licence, and indicate if changes were made. The images or other third party material in this article are included in the article's Creative Commons licence, unless indicated otherwise in a credit line to the material. If material is not included in the article's Creative Commons licence and your intended use is not permitted by statutory regulation or exceeds the permitted use, you will need to obtain permission directly from the copyright holder. To view a copy of this licence, visit http://creativecommons.org/licenses/by/4.0/.

References

- Dickson DW, et al. Office of rare diseases neuropathologic criteria for corticobasal degeneration. J Neuropathol Exp Neurol. 2002;61(11):935–46.
- Flament S, et al. Abnormal Tau proteins in progressive supranuclear palsy. Similarities and differences with the neurofibrillary degeneration of the alzheimer type. Acta Neuropathol. 1991;81(6):591–6.
- Dickson DW. Neuropathologic differentiation of progressive supranuclear palsy and corticobasal degeneration. J Neurol. 1999;246(Suppl 2):II6-15.
- Rosler TW, et al. Four-repeat tauopathies. Prog Neurobiol. 2019;180:101644.
- Graff-Radford J, et al. New insights into atypical Alzheimer's disease in the era of biomarkers. Lancet Neurol. 2021;20(3):222–34.
- Necpal J, Borsek M, Jelenova B. Parkinson's disease on the way to progressive supranuclear palsy: a review on PSP-parkinsonism. Neurol Sci. 2021;42(12):4927–36.
- Hoglinger GU, et al. Clinical diagnosis of progressive supranuclear palsy: the movement disorder society criteria. Mov Disord. 2017;32(6):853-64.
- Constantinides VC, et al. Corticobasal degeneration and corticobasal syndrome: a review. Clin Park Relat Disord. 2019;1:66–71.
- van Eimeren T, et al. Neuroimaging biomarkers for clinical trials in atypical parkinsonian disorders: proposal for a neuroimaging biomarker utility system. Alzheimers Dement (Amst). 2019;11:301–9.
- Whitwell JL, et al. Radiological biomarkers for diagnosis in PSP: where are we and where do we need to be? Mov Disord. 2017;32(7):955-71.
- 11. Scholl M, et al. Distinct 18F-AV-1451 Tau PET retention patterns in early- and late-onset Alzheimer's disease. Brain. 2017;140(9):2286–94.
- Ossenkoppele R, et al. Tau PET patterns mirror clinical and neuroanatomical variability in Alzheimer's disease. Brain. 2016;139(Pt 5):1551–67.
- Coakeley S, et al. Positron emission tomography imaging of Tau pathology in progressive supranuclear palsy. J Cereb Blood Flow Metab. 2017;37(9):3150–60.
- Groot C, et al. Tau PET imaging in neurodegenerative disorders. J Nucl Med. 2022;63(Suppl 1):S20–6.
- Brendel M, et al. Assessment of 18F-PI-2620 as a biomarker in progressive supranuclear palsy. JAMA Neurol. 2020;77(11):1408–19.
- Li CH, et al. Integrated (18)F-T807 Tau PET, structural MRI, and plasma Tau in tauopathy neurodegenerative disorders. Front Aging Neurosci. 2021;13:646440.
- 17. Kunze G, et al. Molecular simulations reveal distinct energetic and kinetic binding properties of [(18)F]PI-2620 on Tau filaments from 3R/4R and 4R tauopathies. ACS Chem Neurosci. 2022;13(14):2222–34.



- Kroth H, et al. Discovery and preclinical characterization of [(18) F]PI-2620, a next-generation Tau PET tracer for the assessment of Tau pathology in Alzheimer's disease and other Tauopathies. Eur J Nucl Med Mol Imaging. 2019;46(10):2178–89.
- Zhou Y, et al. Dissecting the binding profile of PET tracers to corticobasal degeneration Tau fibrils. ACS Chem Neurosci. 2021;12(18):3487–96.
- Franzmeier N, et al. Tau deposition patterns are associated with functional connectivity in primary tauopathies. Nat Commun. 2022;13(1):1362.
- Messerschmidt K, et al. (18)F-PI-2620 Tau PET improves the imaging diagnosis of progressive supranuclear palsy. J Nucl Med. 2022 63:1754–60
- 22. Palleis C, et al. Cortical [(18) F]PI-2620 Binding Differentiates Corticobasal Syndrome Subtypes. Mov Disord. 2021.
- 23. Song M, et al. Binding characteristics of [(18)F]PI-2620 distinguish the clinically predicted Tau isoform in different tauopathies by PET. J Cereb Blood Flow Metab. 2021;41(11):2957–72.
- Kovacs GG, et al. Distribution patterns of Tau pathology in progressive supranuclear palsy. Acta Neuropathol. 2020;140(2):99–119.
- Slemann L, et al. Neuronal and oligodendroglial, but not astroglial, Tau translates to in vivo Tau PET signals in individuals with primary tauopathies. Acta Neuropathol. 2024;148(1):70.
- Schonecker S, et al. Symptomatology in 4-repeat tauopathies is associated with data-driven topology of [(18)F]-PI-2620 tau-PET signal. Neuroimage Clin. 2023;38:103402.
- Malpetti M, et al. Neuroinflammation parallels 18F-PI-2620 positron emission tomography patterns in primary 4-Repeat tauopathies. Mov Disord. 2024;39(9):1480–92.
- Roemer SN, et al. Subcortical tau is linked to hypoperfusion in connected cortical regions in 4-repeat tauopathies. Brain. 2024;147(7):2428–39.
- 29. Leuzy A, et al. Tau PET imaging in neurodegenerative tauopathies-still a challenge. Mol Psychiatry. 2019;24(8):1112–34.
- Bollack A, et al. Longitudinal amyloid and Tau PET imaging in Alzheimer's disease: a systematic review of methodologies and factors affecting quantification. Alzheimers Dement. 2023;19(11):5232–52.
- 31. Braak H, Braak E. Neuropathological stageing of Alzheimerrelated changes. Acta Neuropathol. 1991;82(4):239–59.
- 32. Koga S, et al. Cerebellar ataxia in progressive supranuclear palsy: an autopsy study of PSP-C. Mov Disord. 2016;31(5):653–62.
- Piao YS, et al. Cerebellar cortical tau pathology in progressive supranuclear palsy and corticobasal degeneration. Acta Neuropathol. 2002;103(5):469–74.
- 34. Aguero C, et al. Head-to-head comparison of [(18)F]-Flortaucipir, [(18)F]-MK-6240 and [(18)F]-PI-2620 postmortem binding across the spectrum of neurodegenerative diseases. Acta Neuropathol. 2024;147(1):25.
- Kling A, et al. Exploring the origins of frequent tau-PET signal in vermal and adjacent regions. Eur J Nucl Med Mol Imaging. 2025. https://doi.org/10.1007/s00259-025-07199-x.
- 36. Meindl M, et al. Assessment of [(18)F]PI-2620 Tau-PET quantification via non-invasive automatized image derived input function. Eur J Nucl Med Mol Imaging. 2024;51(11):3252–66.
- Bauer T, et al. Pragmatic algorithm for visual assessment of 4-Repeat tauopathies in [(18)F]PI-2620 PET scans. NeuroImage. 2025;306:121001.
- Song M, et al. Feasibility of short imaging protocols for [(18)F]
 PI-2620 tau-PET in progressive supranuclear palsy. Eur J Nucl Med Mol Imaging. 2021;48(12):3872–85.
- Armstrong MJ, et al. Criteria for the diagnosis of corticobasal degeneration. Neurology. 2013;80(5):496–503.

- Jack CR Jr., et al. Revised criteria for diagnosis and staging of Alzheimer's disease: Alzheimer's association workgroup. Alzheimers Dement. 2024;20(8):5143–69.
- Golbe LI, Ohman-Strickland PA. A clinical rating scale for progressive supranuclear palsy. Brain. 2007;130(Pt 6):1552–65.
- Logan J, et al. Graphical analysis of reversible radioligand binding from time-activity measurements applied to [N-11 C-methyl](-)-cocaine PET studies in human subjects. J Cereb Blood Flow Metab. 1990:10(5):740–7.
- 43. Hammers A, et al. Three-dimensional maximum probability atlas of the human brain, with particular reference to the temporal lobe. Hum Brain Mapp. 2003;19(4):224–47.
- Marotta C, et al. Biomarkers of disease progression in progressive supranuclear palsy for use in clinical trials. Brain Commun. 2025;7(1):fcaf022.
- Rullmann M, et al. Partial-volume effect correction improves quantitative analysis of 18F-Florbetaben beta-Amyloid PET scans. J Nucl Med. 2016;57(2):198–203.
- R Core Team. R: A Language and environment for statistical computing. R Foundation for Statistical Computing; 2021.
- DeLong ER, DeLong DM, Clarke-Pearson DL. Comparing the areas under two or more correlated receiver operating characteristic curves: a nonparametric approach. Biometrics. 1988;44(3):837–45.
- 48. Jack CR Jr., et al. Longitudinal Tau PET in ageing and Alzheimer's disease. Brain. 2018;141(5):1517–28.
- Baker SL, Maass A, Jagust WJ. Considerations and code for partial volume correcting [(18)F]-AV-1451 Tau PET data. Data Brief. 2017;15:648–57.
- Volpi T, et al. An update on the use of image-derived input functions for human PET studies: new hopes or old illusions? EJNMMI Res. 2023;13(1):97.
- 51. Bischof GN, et al. Improved Tau PET SUVR quantification in 4-Repeat Tau phenotypes with [(18)F]PI-2620. J Nucl Med. 2024;65(6):952–5.
- 52. Schöll M, et al. PET imaging of Tau deposition in the aging human brain. Neuron. 2016;89(5):971–82.
- 53. Rullmann M, et al. Multicenter (18)F-PI-2620 PET for in vivo braak staging of tau pathology in Alzheimer's disease. Biomolecules. 2022;12(3):458.
- 54. Jecmenica Lukic M, et al. Copathology in progressive supranuclear palsy: does it matter?? Mov Disord. 2020;35(6):984–93.
- 55. Messerschmidt K, et al. (18)F-PI-2620 Tau PET improves the imaging diagnosis of progressive supranuclear palsy. J Nucl Med. 2022;63(11):1754–60.
- Blazhenets G, et al. [(18)F]PI-2620 binding patterns in patients with suspected alzheimer disease and frontotemporal lobar degeneration. J Nucl Med. 2023;64(12):1980–9.
- Dilcher R, et al. Combining cerebrospinal fluid and PI-2620 tau-PET for biomarker-based stratification of alzheimer's disease and 4R-tauopathies. Alzheimers Dement. 2024;20(10):6896–909.
- 58. Hamasaki H, et al. Tauopathy in basal ganglia involvement is exacerbated in a subset of patients with alzheimer's disease: the Hisayama study. Alzheimers Dement (Amst). 2019;11:415–23.
- Katzdobler S, et al. Additive value of [(18)F]PI-2620 perfusion imaging in progressive supranuclear palsy and corticobasal syndrome. Eur J Nucl Med Mol Imaging. 2023;50(2):423–34.

Publisher's note Springer Nature remains neutral with regard to jurisdictional claims in published maps and institutional affiliations.



Authors and Affiliations

Lukas Frontzkowski^{1,2} · Johannes Gnörich² · Mattes Gross^{1,2} · Amir Dehsarvi¹ · Sebastian N. Roemer-Cassiano^{1,3} · Carla Palleis^{3,4,5} · Sabrina Katzdobler³ · Anna Dewenter¹ · Anna Steward¹ · Davina Biel¹ · Fabian Hirsch¹ · Zeyu Zhu¹ · Johannes Levin^{3,4,5} · Andrew W. Stephens⁶ · Andre Müller⁶ · Norman Koglin⁶ · Gérard N. Bischof⁶ · Gabor G. Kovacs^{7,8} · Günter U. Höglinger^{3,4,5} · Matthias Brendel^{2,4,5} · Nicolai Franzmeier^{1,4,9}

- Lukas Frontzkowski lukas.frontzkowski@med.uni-muenchen.de
- ¹ Institute for Stroke and Dementia Research (ISD), University Hospital, LMU Munich, Feodor-Lynen-Straße 17, Munich 81377, Germany
- Department of Nuclear Medicine, LMU University Hospital, Marchioninistraße 15, Munich 81377, Germany
- Department of Neurology, LMU University Hospital, Munich, Germany
- Munich Cluster for Systems Neurology (SyNergy), Munich, Germany

- ⁵ German Center for Neurodegenerative Diseases (DZNE), Munich, Germany
- 6 Life Molecular Imaging, GmbH, Berlin, Germany
- ⁷ Tanz Centre for Research in Neurodegenerative Disease (CRND), Toronto, Canada
- 8 Laboratory Medicine Program and Krembil Brain Institute, University Health Network, Toronto, Canada
- The Sahlgrenska Academy, Institute of Neuroscience and Physiology, Department of Psychiatry and Neurochemistry, University of Gothenburg, Mölndal and Gothenburg, Sweden

